High-resolution measurements of Mg XI and Cu XX resonance and satellite transitions and the resonance defect in the Mg-pumped Cu x-ray laser scheme

A. Ya. Faenov, B. A. Bryunetkin, V. M. Dyakin, T. A. Pikuz, and I. Yu. Skobelev
Multicharged Ions Spectral Data Center of the National Scientific Research Institute for Physical-technical and Radio-technical Measurements, Mendeleevo, Moscow Region, Russia

S. A. Pikuz
P. N. Lebedev Physical Institute, Leninsky Prospect 53, Moscow, Russia

J. Nilsen, and A. L. Osterheld
Lawrence Livermore National Laboratory, Livermore, California 94551

U. I. Safronova
Institute of Spectroscopy, Troitsk, Moscow Region, Russia
(Received 15 March 1995)

Magnesium and copper plasmas produced by 2-ns pulses of a Nd-glass laser were used to investigate satellite spectra of Li-like Mg X and Na-like Cu XIX and to verify a near resonance between Mg XI and Cu XX transitions, which is the basis of a proposed resonantly photopumped x-ray laser scheme. The emission was measured with a spherical crystal spectrograph that provided high spectral resolution ($\lambda/\Delta\lambda \approx 8000$) and spatial resolution in one dimension. The high resolution allowed improved wavelength measurements for a number of $n=2\rightarrow 1$ Mg X transitions that are satellites to the He-like resonance line, including transitions with $n=3,4$ spectator electrons. Using composite targets, the spatial resolution of the spectrograph enabled highly accurate measurements of $2p$-$4d$ Na-like copper transitions. Collisional-radiative models were used to assist the identification of the Mg X and Cu XIX transitions. Finally, the wavelength difference between the $2p^6$-$(2p^5)_{3/2}4d_{5/2}(J=1)$ Cu XX transition and the $1s^2\ {}^1S_0$–$1s2p^3P_1$ Mg XI intercombination line was measured to be 2.5 ± 0.8 mÅ, with the copper line having a longer wavelength.

PACS number(s): 32.30.Rj, 52.70.La, 42.60.By

I. INTRODUCTION

High-precision wavelength measurements of the K and L spectra of multiply charged ions are very desirable to test methods used for calculating the energy structure of many-electron systems and to investigate practical applications to diagnostics of high-temperature plasma [1,2] and resonantly photopumped x-ray laser schemes [3,4]. Resonance lines of He-like and Ne-like ions and their associated satellite transitions are the most frequently used in spectroscopic diagnostics of plasma. These closed-shell ions produce intense lines over a wide range of plasma conditions and the intensities of the dielectronically excited satellite transitions depend strongly on the electron temperature. In addition, Ne-like ions have played a central role in attempts to develop resonantly photopumped soft-x-ray lasers, because of the simple structure of these ions, their pervasiveness in plasma, and the success of collisionally pumped Ne-like x-ray lasers [5].

Since the original work of Gabriel [6], spectra near the $1s^2\ {}^1S_0$–$1s2p\ {}^1P_1$ resonance line in He-like ions have been widely studied. Many of these spectral lines are produced by $1s^2nl$-$1s2l'nl''$ ($n\geq 2$) satellite transitions in Li-like ions. For $n=2$, these transitions are frequently used for plasma diagnostics [1]. These transitions are sufficiently numerous that many of the observed features are blends and accurate wavelengths of these lines are required for plasma diagnostics. For $n\geq 3$, these satellite lines are frequently unresolved from the resonance line and can affect plasma diagnostics that rely on the width, position, and intensity of the resonance line.

The Na-like satellite transitions to Ne-like resonance lines may also be used to diagnose plasma conditions [7]. Typically, the main problems for high-precision measurements of the wavelengths of L-shell transitions are the absence of good reference lines and the poor spectral resolution of the spectroscopic devices used in the experiments. The need for high resolution is especially important for wavelength measurements of dielectronic satellite transitions to Ne-like ion resonance lines due to their very complicated structure. In our previous investigations, experimental measurements of wavelengths of satellite transitions near Ne-like $n=3\rightarrow 2$ resonance lines were performed for ions with nuclear charge $Z=29$–42 [8–14]. For $n=4\rightarrow 2$ transitions such measurements are now in the initial stage only [15,16].

Resonantly photopumped x-ray laser schemes require that the wavelengths of the pumping and absorbing transitions overlap to 1 part in several thousand. In general, this is beyond the accuracy of wavelength calculations for transitions in multielectron ions and the degree of overlap must be tested experimentally. Many of the most accurate wavelength measurements of transitions involved in resonantly photopumped x-ray laser schemes have been obtained by using the electron-beam ion trap (EBIT) [17] as a spectroscopic source. Using the EBIT, the wavelengths of some spectral transitions of Ne-like ions have been measured with a very high accuracy of up to 50 parts per million [18]. However,

not all transitions are easily measured in EBIT installations, where the brightest transitions are generally produced by direct collisional excitation from the ground state. In addition, experiments in high-density plasmas can study the effects of line shapes, plasma shifts, and bulk plasma motion, which may be present in the x-ray laser plasma.

In the present work a high-resolution spectrograph ($\lambda/\Delta\lambda \approx 8000$) is used with composite targets to investigate magnesium K-shell and copper L-shell satellite structures and to evaluate a line resonance that is the basis of a proposed magnesium-pumped copper x-ray laser. The high resolution of the spectrograph allowed us to resolve and to improve the accuracy of wavelength measurements for transitions in Li-like Mg XI, including a number of high-n satellite transitions. Precise measurements of the wavelengths and a theoretical interpretation of satellite lines near the $2p^6$-$(2p^5)_{3/2}4d_{5/2}(J=1)$ transition in Ne-like Cu XX are presented. These measurements will improve the application of these transitions to plasma diagnostics. Finally, the spatial resolution of the spectrograph was used to measure the resonance defect of the intercombination line of He-like Mg XI and the $2p^6$-$(2p^5)_{3/2}4d_{5/2}(J=1)$ line in Ne-like Cu XX. This pair of lines is very attractive for a potential x-ray laser scheme based on resonant photopumping [4].

II. EXPERIMENTAL ARRANGEMENT

The experiments were performed at the Nd-glass laser facility at the Multicharged Ions Spectral Data Center of the National Scientific Research Institute for Physical-technical and Radio-technical Measurements in Mendeleevo, Russia. The scheme of the experiment is shown in Fig. 1. Pulses of light from an Nd-glass laser with energy up to 30 J and duration of 2 ns at half maximum were focused by a two-component objective onto the surface of massive targets made of magnesium and copper. We used a target in the form of a step in which the surface of a magnesium plate was raised by about 0.3 mm relative to the copper target. The x-ray emission spectra of the plasma were recorded on DEF-2 film with the aid of a high-resolution spectrograph with a spherical mica crystal ($2d \approx 19.9$ Å) with a radius of 250 mm. To achieve higher spectral resolution the spectra were registered in the second order of reflection of the mica crystal. The film was exposed in two stages: the spectrum of the copper plasma was recorded first and then, after this target was moved in the horizontal direction, the spectrum of the magnesium plasma was recorded on the same film. The spectrograph was used in a vertical focusing configuration, focusing crystal spectrometer with one-dimensional spatial resolution (FSSR-1D) [19–21] and as a result the spectra were obtained with spatial resolution in the direction of the plasma expansion as shown in Fig. 1. The spatial resolution allowed the K-shell Mg lines to be used as standard wavelengths for the analysis of the copper spectra and enabled a direct measurement of the degree of overlap in the magnesium-pumped copper x-ray laser scheme.

III. RESULTS AND INTERPRETATION

Densitometer traces of the spectra emitted by the magnesium and copper plasmas in the spectra region 9.15–9.33 Å

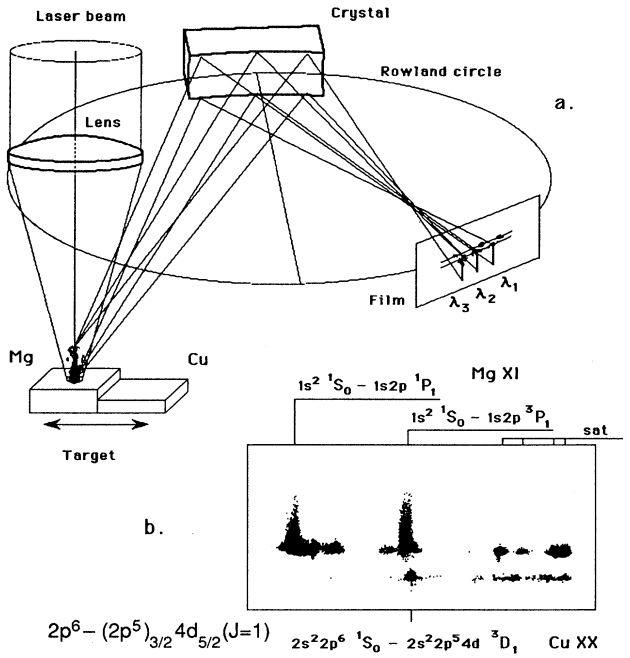

FIG. 1. (a) Scheme of the experiment showing the geometry of the composite target and the FSSR-1D focusing spectrograph used for registration of x-ray spectra with one-dimensional spatial resolution. (b) Example of the film image obtained by the FSSR-1D spectrograph after a two-shot exposure. The target was moved in the horizontal direction between laser shots.

are reproduced in Fig. 2. In the first stage of the experiments, wavelengths of Li-like satellites in the vicinity of the Mg XI resonance and intercombination lines were measured. The dispersion curve of the spectrograph was determined by using theoretical wavelengths for the resonance line of Mg XI at 9.1689 Å [22] and the j satellite line at 9.3206 Å, calculated by the $1/Z$ expansion method using the MZ computer code [23,24], as reference wavelengths. (In the present work, Li-like KLL satellite transitions are designated by the notation of Gabriel [6].) Noting that lines separated in wavelength by approximately 1 mÅ are observed as separate peaks, the spectral resolution is estimated as $\lambda/\Delta\lambda \approx 8000$. This resolution and the uncertainty in the determination of the peak positions give a random error in the wavelength determination of about ± 0.8 mÅ.

A. Li-like Mg satellite transitions

As noted above, the $n=2 \rightarrow 1$ resonance and satellite transitions in He-like and Li-like ions have been widely used for diagnostics of a variety of plasma sources [1,2]. The most useful Li-like satellite lines for plasma diagnostics are the $1s^22l$-$1s2l'2l''$ transitions because they are the most easily resolved from the He-like transitions. However, there are additional satellite lines of the type $1s^2nl$-$1s2l'nl''$, where $n \geq 3$, which are frequently not resolved from the $1s^2$–$1s2p^1P_1$ resonance line (for high enough values of n, these are never resolved). These blended transitions produce temperature- and density-dependent contributions to the apparent intensity, width, and central frequency of the reso-

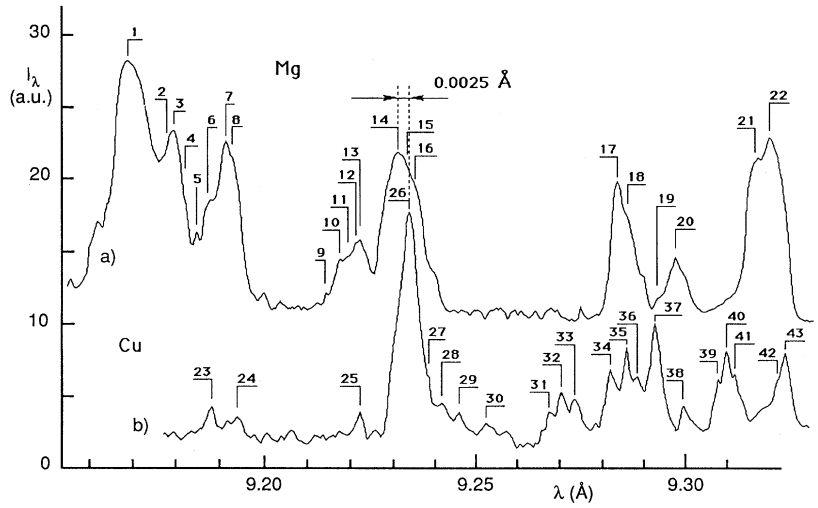

FIG. 2. Densitometer traces of the experimental spectra emitted by the magnesium and copper plasmas. The resonant line overlap is clearly seen.

nance line and thus affect diagnostics of the plasma conditions, ion temperature, and bulk plasma velocity. These transitions have been investigated in medium-Z elements in tokamak and EBIT experiments [25–29], but have not been systematically studied in higher-density plasmas formed from light ions (e.g., aluminum and magnesium), such as those commonly produced in laser-produced plasma experiments [30]. Decaux *et al.* [28] showed that electron temperatures inferred from Li-like iron satellite to resonance line ratios differed by up to 20%, depending on the theoretical values used for the wavelengths of the high-n transitions. This indicates that the position of these satellites must be experimentally determined.

The magnesium transitions in the present experiments were identified with the aid of a theoretical simulation of the shape of the spectrum. A quasistationary, collisional-radiative model was used to calculate the intensities of the resonance and intercombination lines of He-like Mg XI and the satellite lines caused by $1s2lnl'$-$1s^2nl''$ transitions in Li-like Mg X, for $n=2\rightarrow4$. For the $1s2l2l'$ levels, the two main population mechanisms (dielectronic capture $1s^2+e^-\rightarrow1s2l2l'$ and innershell excitation $1s^22l+e^-\rightarrow1s2l2l'+e^-$) were taken into account. It was assumed that the more highly excited $1s2lnl'$ ($n=3,4$) levels are populated only by the dielectronic capture process. The transition wavelengths, probabilities of radiative and autoionization decays, and electron-impact excitation rates were taken from [31,32].

The emission spectrum of He-like and Li-like magnesium ions for the spectral band 9.15–9.33 Å obtained from the theoretical calculations is compared to the experimental spectrum in Fig. 3. It was assumed that all lines have Gaussian shapes. The values of electron plasma temperature $T_e=260$ eV, electron density $N_e=2\times10^{20}$ cm^{-3}, and ratio of Li-like and He-like ion densities $N(\mathrm{Li})/N(\mathrm{He})=0.22$ were chosen to obtain the best agreement between the theoretical and experimental spectra.

The line identifications and experimentally determined wavelengths are summarized in Table I. The observed transitions are numbered as in Figs. 2 and 3. The measured Li-like wavelengths are compared in Table I to theoretical calculations performed with the YODA computer code [33], which were slightly shifted using the approach outlined in [24,34], as well as the calculations performed with the MZ computer code [23,24]. The measured He-like wavelengths

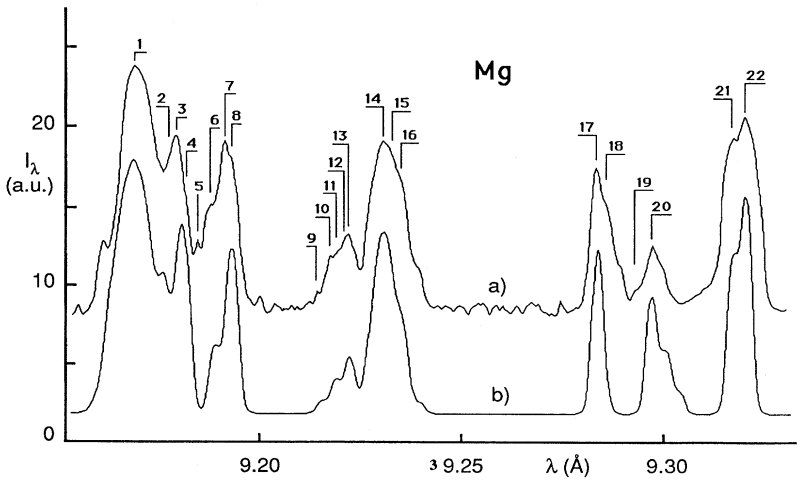

FIG. 3. Comparison of (a) a densitogram of the experimental spectrum of the magnesium plasma and (b) the results of a model calculation assuming $T_e=260$ eV, $N_e=2\times10^{20}$ cm^{-3}, and $N_{\mathrm{Li}}/N_{\mathrm{He}}=0.22$.

TABLE I. Experimental and theoretical wavelengths of He-like and Li-like magnesium transitions identified in the present experiments. The transitions are numbered as in Fig. 3 and the lower case letters in parentheses in the transition designation are from the notation of Gabriel [6].

Index	λ_{expt} (Å)	Transition	λ_{MZ}[a] (Å)	λ_{YODA}[b] (Å)	λ[c] (Å)	λ[d] (Å)
1	9.1689[e]	$1s^2\ ^1S_0$–$1s2p\ ^1P_1$ (w)	9.1696	9.1686	9.1689	9.1688
2	9.1764	$1s^24d\ ^2D_{3/2}$–$1s2p(^1P)4d\ ^2F_{5/2}$	9.1761	9.1731		
		$^2D_{5/2}$-$^2F_{5/2}$	9.1762	9.1732		
		$^2D_{5/2}$-$^2F_{7/2}$	9.1766	9.1736		
3	9.1780	$1s^23d\ ^2D_{3/2}$–$1s2p(^1P)3d\ ^2F_{5/2}$	9.1796	9.1753		
4	9.1801	$1s^24p\ ^2P_{1/2}$–$1s2p(^1P)4p\ ^2D_{3/2}$	9.1806	9.1787		
		$^2P_{3/2}$-$^2D_{5/2}$	9.1808	9.1787		
5	9.1817	$1s^23d\ ^2D_{5/2}$–$1s2p(^1P)3d\ ^2F_{7/2}$	9.1811	9.1768		
6	9.1863	$1s^23s\ ^2S_{1/2}$–$1s2p(^1P)3s\ ^2P_{1/2}$	9.1886	9.1863		
		$^2S_{1/2}$-$^2P_{3/2}$	9.1894	9.1871		
7	9.1908	$1s^23p\ ^2P_{3/2}$–$1s2p(^1P)3p\ ^2P_{3/2}$	9.1923	9.1915		
8	9.1919	$1s^23p\ ^2P_{1/2}$–$1s2p(^1P)3p\ ^2D_{3/2}$	9.1927	9.1918		
		$^2P_{3/2}$-$^2D_{5/2}$	9.1938	9.1924		
9	9.2136					
10	9.2165	$1s^23s\ ^2S_{1/2}$–$1s2p(^3P)3s\ ^2P_{3/2}$	9.2157	9.2146		
11	9.2186	$1s^22p\ ^2P_{1/2}$–$1s(2p^2\ ^1S)\ ^2S_{1/2}$ (n)	9.2189	9.2127		
		$1s^23s\ ^2S_{1/2}$–$1s2p(^3P)3s\ ^2P_{1/2}$	9.2191	9.2180		
12	9.2207	$1s^23p\ ^2P_{3/2}$–$1s2p(^3P)3p\ ^2S_{1/2}$	9.2207	9.2134		
13	9.2219	$1s^22p\ ^2P_{3/2}$–$1s(2p^2\ ^1S)^2S_{1/2}$ (m)	9.2223	9.2160		
14	9.2318	$1s^2\ ^1S_0$–$1s2p\ ^3P_1$ (y)	9.2314	9.2332	9.2310	9.2312
15	9.2340	$1s^22s\ ^2S_{1/2}$–$1s(2s2p\ ^1P)^2P_{3/2}$ (s)	9.2355	9.2308		
16	9.2351	$1s^22s\ ^2S_{1/2}$–$1s(2s2p\ ^1P)^2P_{1/2}$ (t)	9.2360	9.2314		
17	9.2840	$1s^22s\ ^2S_{1/2}$–$1s(2s2p\ ^3P)^2P_{3/2}$ (q)	9.2844	9.2834		
18	9.2865	$1s^22s\ ^2S_{1/2}$–$1s(2s2p\ ^3P)^2P_{1/2}$ (r)	9.2863	9.2854		
19	9.2935	$1s^22p\ ^2P_{1/2}$–$1s(2p^2\ ^3P)^2P_{3/2}$ (b)	9.2947	9.2946		
20	9.2976	$1s^22p\ ^2P_{1/2}$–$1s(2p^2\ ^3P)^2P_{1/2}$ (d)	9.2980	9.2979		
		$1s^22p\ ^2P_{3/2}$–$1s(2p^2\ ^3P)^2P_{3/2}$ (a)	9.2982	9.2979		
21	9.3166	$1s^22p\ ^2P_{1/2}$–$1s(2p^2\ ^1D)^2D_{3/2}$ (k)	9.3161	9.3154		
22	9.3206[f]	$1s^22p\ ^2P_{3/2}$–$1s(2p^2\ ^1D)^2D_{5/2}$ (j)	9.3206	9.3195		

[a]Calculated for present work using the MZ code [23,24].
[b]Calculated using YODA code [33], using the method described in [24,34].
[c]From [22].
[d]From [35].
[e]Reference line, from [22].
[f]Reference line, from [23,24].

are also compared to theoretical results from Refs. [22] and [35]. It is clearly seen from Table I and Fig. 3 that there is very good agreement between the theoretical and experimental intensities of the satellite transitions, including lines caused by the $1s^23l$-$1s2l'3l''$ and $1s^24l$-$1s2l'4l''$ transitions. These results improve upon existing wavelength measurements for these transitions, particularly for the high-n satellites, and will lead to improved models of magnesium emission for plasma diagnostics.

B. Na-like Cu XX satellite transitions

The $n=3\rightarrow2$ Na-like satellite transitions were used for plasma diagnostics in Ref. [7] and further studied in [8–14]. More recently, the $n=4\rightarrow2$ satellite transitions have been investigated [15,16]. The $n=4\rightarrow2$ transitions may be more favorable than the $n=3\rightarrow2$ transitions for diagnostics, primarily because they have lower optical depths and are more spectrally isolated. While the spectrum of these L-shell transitions are much more complex than for K-shell satellites, the development of accurate emission models for these ions will provide opportunities to diagnose plasmas, such as collisionally pumped x-ray laser plasmas, which predominantly contain L-shell ions. The high resolution of the present measurements provides an important test of the models of the very complex L-shell satellite emission.

The brightest lines in the $n=4\rightarrow2$ spectrum of Ne-like ions are the $2p^6$-$(2p^5)_{3/2}4d_{5/2}(J=1)$ and $2p^6$-$(2p^5)_{1/2}4d_{3/2}(J=1)$ transitions. The 9.16–9.33 Å spectral region investigated here contains the $2p^6$-$(2p^5)_{3/2}4d_{5/2}(J=1)$ transition and Na-like transitions, which are predominantly satellites to the $2p^6$-$(2p^5)_{1/2}4d_{3/2}(J=1)$ transition at 9.104 Å, which was not measured in these experiments.

The dispersion curve determined in the analysis of the magnesium spectra described above was used to measure the

TABLE II. Experimental and theoretical wavelengths of Ne-like and Na-like copper transitions identified in the present experiments. The transitions are numbered as in Fig. 4. In the transition designation, the bar over the $2p$ indicates a single hole, and unspecified inner shells are completely filled. The theoretical wavelengths are from the HULLAC atomic code package.

Index	λ_{expt} (Å)	λ_{theor} (Å)	Transition
23	9.1872		
24	9.1921	9.1924	$3p_{3/2}$-$[(\overline{2p}_{3/2}3d_{3/2})_3 4f_{5/2}]_{5/2}$
25	9.2239		
26	9.2343	9.2340	$2s^2 2p^6$-$(\overline{2p}_{3/2}4d_{5/2})_1$
27	9.2393		
28	9.2429		
29	9.2469	9.2467	$3d_{3/2}$-$[(\overline{2p}_{1/2}3d_{3/2})_1 4d_{5/2}]_{3/2}$
30	9.2526	9.2513	$3d_{5/2}$-$[(\overline{2p}_{1/2}3d_{3/2})_1 4d_{5/2}]_{3/2}$
		9.2542	$3d_{3/2}$-$[(\overline{2p}_{1/2}3d_{3/2})_1 4d_{3/2}]_{3/2}$
31	9.2690	9.2680	$3d_{3/2}$-$[(\overline{2p}_{1/2}3d_{3/2})_1 4d_{3/2}]_{5/2}$
32	9.2710	9.2727	$3d_{5/2}$-$[(\overline{2p}_{1/2}3d_{3/2})_1 4d_{3/2}]_{5/2}$
33	9.2742	9.2742	$3s_{1/2}$-$[(\overline{2p}_{3/2}3p_{3/2})_2 4p_{1/2}]_{3/2}$
		9.2747	$3p_{1/2}$-$[(\overline{2p}_{1/2}3p_{3/2})_1 4d_{3/2}]_{1/2}$
34	9.2829	9.2825	$3p_{3/2}$-$[(\overline{2p}_{1/2}3p_{3/2})_2 4d_{3/2}]_{1/2}$
		9.2828	$3p_{3/2}$-$[(\overline{2p}_{3/2}3d_{3/2})_0 4p_{1/2}]_{1/2}$
		9.2847	$3p_{1/2}$-$[(\overline{2p}_{1/2}3p_{3/2})_1 4d_{3/2}]_{3/2}$
35	9.2865	9.2862	$3s_{1/2}$-$[(\overline{2p}_{1/2}3s_{1/2})_1 4d_{3/2}]_{1/2}$
		9.2863	$3s_{1/2}$-$[(\overline{2p}_{1/2}3s_{1/2})_1 4d_{3/2}]_{3/2}$
36	9.2889	9.2880	$3s_{1/2}$-$[(\overline{2p}_{3/2}3p_{3/2})_1 4p_{3/2}]_{3/2}$
37	9.2936	9.2919	$3p_{3/2}$-$[(\overline{2p}_{1/2}3p_{3/2})_2 4d_{3/2}]_{3/2}$
		9.2946	$3p_{3/2}$-$[(\overline{2p}_{1/2}3p_{3/2})_1 4d_{3/2}]_{5/2}$
		9.2955	$3p_{3/2}$-$[(\overline{2p}_{1/2}3p_{3/2})_1 4d_{5/2}]_{3/2}$
38	9.3004	9.3022	$3p_{1/2}$-$[(\overline{2p}_{1/2}3p_{1/2})_1 4d_{3/2}]_{1/2}$
39	9.3085	9.3062	$3d_{5/2}$-$[(\overline{2p}_{1/2}3d_{5/2})_3 4d_{3/2}]_{3/2}$
		9.3092	$3d_{3/2}$-$[(\overline{2p}_{1/2}3d_{5/2})_3 4d_{3/2}]_{5/2}$
		9.3097	$3d_{5/2}$-$[(\overline{2p}_{1/2}3d_{5/2})_2 4d_{3/2}]_{7/2}$
40	9.3107	9.3105	$3d_{3/2}$-$[(\overline{2p}_{1/2}3d_{3/2})_2 4d_{3/2}]_{1/2}$
		9.3108	$3p_{1/2}$-$[(\overline{2p}_{1/2}3p_{1/2})_1 4d_{3/2}]_{3/2}$
41	9.3130	9.3136	$3s_{1/2}$-$[(\overline{2p}_{1/2}3s_{1/2})_0 4d_{3/2}]_{3/2}$
		9.3140	$3d_{5/2}$-$[(\overline{2p}_{1/2}3d_{5/2})_3 4d_{3/2}]_{5/2}$
		9.3154	$3d_{5/2}$-$[(\overline{2p}_{1/2}3d_{5/2})_2 4d_{3/2}]_{3/2}$
		9.3159	$3p_{3/2}$-$[(\overline{2p}_{1/2}3p_{3/2})_1 4d_{3/2}]_{3/2}$
42	9.3218	9.3207	$3d_{5/2}$-$[(\overline{2p}_{1/2}3d_{5/2})_2 4d_{5/2}]_{7/2}$
43	9.3236	9.3237	$3d_{5/2}$-$[(\overline{2p}_{1/2}3d_{5/2})_2 4d_{3/2}]_{5/2}$
		9.3252	$3d_{3/2}$-$[(\overline{2p}_{1/2}3d_{3/2})_2 4d_{3/2}]_{5/2}$

wavelengths in the spectrum of the copper plasma. As in the case of the magnesium spectrum, the copper satellite transitions were identified with the aid of a theoretical calculation of the emitted spectrum. The following processes were taken into account for the $3l4l'$ Na-like levels:

$$2s^2 2p^6 + e^- \rightarrow \begin{cases} 2s^2 2p^5 3l4l' \\ 2s^1 2p^6 3l4l' \end{cases}$$

(dielectronic recapture),

$$2s^2 2p^6 nl'' + e^- \rightarrow \begin{cases} 2s^2 2p^5 3l4l' + e^- \\ 2s^1 2p^6 3l4l' + e^- \end{cases}$$

(inner-shell excitation),

where $n=3,4$ and $l,l',l'' \leq n-1$. All autoionization and radiative decays were included, as well as all collisional mixing rates. The atomic parameters were taken from the Hebrew University–Lawrence Livermore Atomic Code package (HULLAC). In the atomic structure code, the wave functions, energy levels, and radiative and autoionization rates were obtained from a fully relativistic configuration-interaction treatment based on a parametric potential model [36,37] and the distorted-wave approximation is used for the collisional transition rates [38]. A more detailed description of the theoretical calculations is given in [15].

The experimental spectrum is compared in Fig. 4 to the theoretical spectrum, assuming $T_e=260$ eV and $N_e=2\times10^{20}$ cm^{-3}, as in Fig. 3. The experimental wavelengths are listed in Table II, along with the proposed line identifications. As shown in Fig. 4, the experimental and theoretical data are in good agreement. Some experimentally determined lines are not identified. The transitions may arise from $2p^5 4lnl'$ levels, where $n \geq 4$, or from transitions in other ionization sequences. Also, the level designations in Table II are based on the dominant jj-coupled levels contributing to the physical states in the atomic-structure calculations. Since the doubly excited Na-like levels are highly numerous and closely spaced in energy, a strong configuration interaction occurs. Thus some transitions in Table II appear to be two-electron transitions.

C. Line overlap measurement

The resonantly photopumped x-ray laser scheme proposed in [4] relies on a potential resonance between the Mg XI intercombination transition and the $2p^6$-$(2p^5)_{3/2}4d_{5/2}(J=1)$ Cu XX transition. In this scheme, the $(2p^5)_{3/2}4d_{5/2}(J=1)$ level is pumped by the magnesium emission. Cascades from this level strongly enhance the populations of $2p^5 3p$ metastable levels, producing inversion on $3p$-$3s$ transitions near 300 Å. The viability of the scheme requires that the difference between the pumping and absorbing transitions is small compared to their linewidths. Assuming an ion temperature of 400 eV—a typical electron temperature where these ions are abundant—the copper and magnesium lines will have Doppler widths of 2 and 3 mÅ, respectively. Opacity and plasma broadening in a realistic x-ray laser plasma would further increase the width of the pumping transition.

The wavelength difference between the $2p^6$-$(2p^5)_{3/2}4d_{5/2}(J=1)$ Cu XX and the $1\,^1S_0$–$2\,^3P_1$ Mg XI lines was measured to be 2.5 ± 0.8 mÅ, with the copper line at a longer wavelength. Note that this difference was measured directly and does not depend on a precise calibration of the spectrograph. Thus the required line overlap exists, suggesting that this scheme should be pursued experimentally. Our result is in good agreement with a previous measurement of 1.9 ± 0.7 mÅ using the EBIT facility [39]. We note that the degree of line overlap in our experiments is measured under conditions that are closer to the real experimental conditions for x-ray lasing.

IV. CONCLUSION

We have measured (with an uncertainty of 0.8 mÅ) a number of satellite transitions in two ionic systems relevant

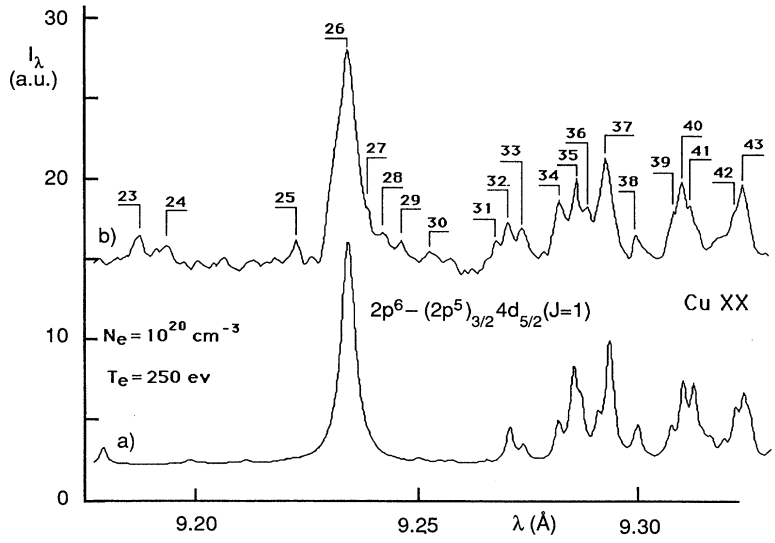

FIG. 4. Comparison of (a) a densitogram of the experimental spectrum of the copper plasma and (b) the results of a model calculation assuming $T_e = 260$ eV and $N_e = 2 \times 10^{20}$ cm^{-3}.

to plasma diagnostics and evaluated a potential line overlap that forms the basis of a proposed resonantly photopumped x-ray laser. We have improved identifications and wavelength measurements of $1s^2nl$-$1s2l'nl''$ transitions in Li-like Mg X, where $n=2\rightarrow4$. The high resolution of the present measurements allowed us to identify a number of such transitions with $n=3,4$, which are typically not resolved from the He-like resonance line for light ions such as magnesium. These transitions play an important role in modifying the use of the satellite and resonance lines for plasma diagnostics.

We have also identified a number of $2p^6$-$2p^5 3l4l'$ Na-like Cu IX satellite transitions between 9.15 and 9.33 Å. These L-shell satellite transitions can be used for plasma diagnostics in the same manner as K-shell satellites and the successful modeling of these lines provides opportunities to diagnose plasmas containing Ne-like ions, such as Ne-like x-ray laser plasmas.

Finally, the resonance defect between the $1s^2\ ^1S_0$–$1s2p\ ^3P_1$ Mg XI intercombination line and the $2p^6$-$(2p^5)_{3/2}4d_{5/2}(J=1)$ Cu XX line at 9.2343 Å was determined to be 2.5 ± 0.8 mÅ, with the copper line at a longer wavelength. This measurement supports the potential of this line pair to achieve x-ray lasing on the basis of the resonant photopumping scheme.

ACKNOWLEDGMENT

This work was performed in part under the auspices of the U.S. Department of Energy by Lawrence Livermore National Laboratory under Contract No. W-7405-Eng-48.

[1] V.A. Boiko, *et al.*, J. Sov. Laser Res. **6**, 85 (1985).

[2] V.A. Boiko, V.G. Palchikov, I. Yu. Skobelev, and A .Ya. Faenov, *X-Ray Spectroscopy of Multiply Charged Ions* (Energoatomizdat, Moscow, 1988).

[3] R.C. Elton, *X-Ray Lasers* (Academic, New York, 1990).

[4] J. Nilsen, Opt. Commun. **78**, 51 (1990).

[5] D.L. Matthews, P.L. Hagelstein, M.D. Rosen, M.J. Eckart, N.M. Ceglio, A.U. Hazi, H. Medecki, B.J. MacGowan, J.E. Trebes, B.L. Whitten, E.M. Campbell, C.W. Hatcher, A.M. Hawryluk, R.L. Kauffman, L.D. Pleasance, G. Rambach, J.H. Scofield, G. Stone, and T.A. Weaver, Phys. Rev. Lett. **54**, 110 (1985).

[6] A.H. Gabriel, Mon. Not. R. Astron. Soc. **160**, 89 (1972).

[7] W.H. Goldstein, R.S. Walling, J. Bailey, M.H. Chen, R. Fortner, M. Klapisch, T. Phillips, and R.E. Stewart, Phys. Rev. Lett. **58**, 2300 (1987).

[8] J. Nilsen, S.A. Pikuz, I. Yu. Skobelev, A.Ya. Faenov, S.Ya. Khakhalin, B.K. Khabibulaev, and Sh. A. Ermatov, Kvant. Elektron. **20**, 1164 (1993) [Quantum Electron. **23**, 1010 (1993)].

[9] J. Nilsen, S.A. Pikuz, I. Yu. Skobelev, A.Ya. Faenov, and S.Ya. Khakhalin, Izm. Tekh. **5**, 3 (1994) [Meas. Tech. **37**, 477 (1994)].

[10] B.A. Bryunetkin, V.M. Dyakin, J. Nilsen, I.Yu. Skobelev, S.A. Pikuz, A.Ya. Faenov, and S.Ya. Khakhalin, Kvant. Elektron. **21**, 137 (1994) [Quantum Electron. **24**, 133 (1994)].

[11] S.Ya. Khakhalin, B.A. Bryunetkin, I.Yu. Skobolev, A.Ya. Faenov, J. Nilsen, A. Osterheld, and S.A. Pikuz, Zh. Éksp. Teor. Fiz. **105**, 1181 (1994) [Sov. Phys. JETP **78**, 633 (1994)].

[12] S. Ya. Khakhalin, A.Ya. Faenov, I. Yu. Skobelev, S.A. Pikuz, J. Nilsen, and A. Osterheld, Phys. Scr. **50**, 102 (1994).

[13] S.Ya. Khakhalin, V.M. Dyakin, A.Ya. Faenov, H. Fiedorowicz, A. Bartnik, P. Parys, J. Nilsen, and A. Osterheld, Phys. Scr. **50**, 106 (1994).

[14] A.R. Mingaleev, S.A. Pikuz, V.M. Romanova, T.A. Shelkovenko, A.Ya. Faenov, S.A. Ermatov, and J. Nilsen, Kvant. Elektron. **20**, 461 (1993) [Quantum Electron. **23**, 397 (1993)].

[15] A.L. Osterheld, J. Dunn, B.K.F. Young, S.B. Libby, A. Szoke, R.S. Walling, W.H. Goldstein, R.E. Stewart, A.Ya. Faenov, I.Yu. Skobelev, and S.Ya. Khakhalin, in *X-Ray Lasers 1994*,

Fourth International Colloquium, Williamsburg, VA, edited by D.C. Eder and D.L. Matthews, AIP Conf. Proc. No. 332 (AIP, New York, 1994), p. 215.
[16] S.Ya. Khakhalin, V.M. Dyakin, A.Ya. Faenov, H. Fiedorowicz, A. Bartnik, P. Parys, A. Osterheld, and J. Nilsen, J. Opt. Soc. Am. B **12**, 1203 (1995).
[17] M.A. Levine *et al.*, Nucl. Instrum. Methods Phys. Res. Sect. B **43**, 431 (1989).
[18] J. Nilsen, P. Beiersdorfer, S.R. Elliott, and A.L. Osterheld, Phys. Scr. **47**, 42 (1993).
[19] A.Ya. Faenov *et al.*, Proc. SPIE Int. Soc. Opt. Eng. **2015**, 64 (1993).
[20] A.Ya. Faenov, S.A. Pikuz, A.I. Erko, B.A. Bryunetkin, V.M. Dyakin, G.V. Ivanenko, A.R. Mingaleev, T.A. Pikuz, V.M. Romanova, and T.A. Shelkovenko, Phys. Scr. **50**, 333 (1994).
[21] J. Nilsen, P. Beiersdorfer, S.R. Elliott, T.W. Phillips, B.A. Bryunetkin, V.M. Dyakin, T.A. Pikuz, A.Ya. Faenov, S.A. Pikuz, S. von Goeler, M. Bitter, P.A. Loboda, V.A. Lykov, and V.Yu. Politov, Phys. Rev. A **50**, 2143 (1994).
[22] V.A. Boiko, V.G. Palchikov, I. Yu. Skobelev, and A.Ya. Faenov, *Spectroscopic Constants of Atoms and Ions* (Izdatel'stvo Standart, Moscow, 1988).
[23] V.P. Shevelko and L.A.Vainstein, *Atomic Physics for Hot Plasmas* (Institute of Physics, Bristol, 1993).
[24] J. Nilsen and U.I. Safronova, J. Quant. Spectrosc. Radiat. Transfer **49**, 371 (1993).
[25] F. Bely-Dubau, A.H. Gabriel, and S. Volante, Mon. Not. R. Astron. Soc. **189**, 801 (1979).
[26] M. Bitter, S. von Goeler, K.W. Hill, R. Horton, D. Johnson, W. Roney, N. Sautohoff, E. Silver, and W. Stodiek, Phys. Rev. Lett. **47**, 921 (1981).
[27] K.R. Karim and C.P. Bhalla, Phys. Rev. A **43**, 615 (1991).
[28] V. Decaux, M. Bitter, H. Hsuan, K.W. Hill, S. von Goeler, H. Park, and C.P. Bhalla, Phys. Rev. A **32**, 3011 (1985).
[29] P. Beiersdorfer, M.B. Schneider, M. Bitter, and S. von Goeler, Rev. Sci. Instrum. **63**, 5029 (1992).
[30] R. Kauffman, in *Physics of Laser Plasma* (North-Holland, Amsterdam, 1991), Vol. 3.
[31] U.I. Safronova, A.M. Urnov, and L.A. Vainshtein, P.N. Lebedev Physical Institute Report No. N212, 1978 (unpublished).
[32] L.A. Vainshtein and U.I. Safronova, *Correlation and Relativistic Effects in Atoms and Ions* (Scientific Council of Spectroscopy, Soviet Academy of Sciences, Moscow, 1986), p. 190.
[33] P.L. Hagelstein and R.K. Jung, At. Data Nucl. Data Tables **37**, 121 (1987).
[34] U.I. Safronova and J. Nilsen, J. Quant. Spectrosc. Radiat. Transfer **51**, 853 (1994).
[35] G.W. Drake, Can. J. Phys. **66**, 586 (1988).
[36] M. Klapisch, J. L. Schwob, B.S. Fraenkel, and J. Oreg, J. Opt. Soc. Am. **61**, 148 (1977).
[37] J. Oreg, W.H. Goldstein, M. Klapisch, and A. Bar-Shalom, Phys. Rev. A **44**, 1750 (1991).
[38] A. Bar-Shalom, M. Klapisch, and J. Oreg, Phys. Rev. A **38**, 1773 (1988).
[39] P. Beiersdorfer, S.R. Elliot, and J. Nilsen, Phys. Rev. A **49**, 3123 (1994).